THE JOURNAL OF PHYSICAL CHEMISTRY LETTERS
A JOURNAL OF THE AMERICAN CHEMICAL SOCIETY

pubs.acs.org/JPCL

Letter

# Nitrile Vibrational Lifetimes as Probes of Local Electric Fields

Philip A. Kocheril, Haomin Wang, Dongkwan Lee, Noor Naji, and Lu Wei*

Cite This: J. Phys. Chem. Lett. 2024, 15, 5306−5314

Read Online

ACCESS | Metrics & More | Article Recommendations | Supporting Information

**ABSTRACT:** Optical measurements of electric fields have wide-ranging applications in the fields of chemistry and biology. Previously, such measurements focused on shifts in intensity or frequency. Here, we show that nitrile vibrational lifetimes can report local electric fields through ultrasensitive picosecond mid-infrared−near-infrared double-resonance fluorescence spectro-microscopy on Rhodamine 800. Using a robust convolution fitting approach, we observe that the nitrile vibrational lifetimes are strongly linearly correlated ($R^2$ = 0.841) with solvent reaction fields. Supported by density functional theory, we rationalize this trend through a doorway model of intramolecular vibrational energy redistribution. This work provides new fundamental insights into the nature of vibrational energy flow in large polyatomic molecular systems and establishes a theoretical basis for electric field sensing with vibrational lifetimes, offering a new experimental dimension for probing intracellular electrostatics.

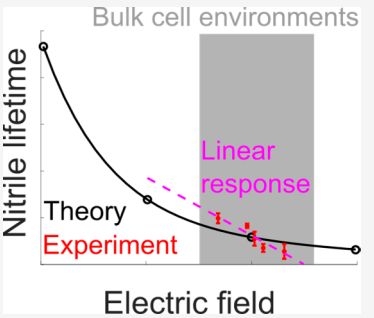




Electric fields are central to many aspects of the physical sciences, including chemical reactivity, cell signaling, and more.[1−8] Over 100 years ago, Stark reported that electric fields can affect how atoms and molecules interact with light; in particular, he observed that degenerate spectral lines in hydrogen are split into multiple components in a strong electric field.[9] This phenomenon is now called the Stark effect and provides useful information across much of the electromagnetic spectrum.[10−12] For example, electric fields almost fully break degeneracy in gas-phase microwave rotational spectroscopy, facilitating detailed spectral assignments that provide fundamental understanding of molecular structure and geometry.[13−15] The electronic Stark effect is the physical basis for sensing cellular potentials with electrochromic dyes, whose fluorescence emission spectra are influenced by the local electric field.[16] Electric field sensing has broad-ranging applications in molecular biology, from characterizing enzyme active sites to mapping spatially heterogeneous hydration.[17−20]

Rotational and electronic Stark effect spectroscopy present extreme cases of a trade-off between quantitative interpretability and biological applicability. The theoretical description of the rotational Stark effect is robust, but microwave spectroscopy methods are incompatible with aqueous biochemical samples.[21,22] In contrast, the electronic Stark effect can qualitatively characterize intracellular electric fields, but the response of a fluorescent emission profile to an applied field is rarely linear and immensely challenging to predict.[5,6,23] Over the years, the vibrational Stark effect emerged as a highly promising spectroscopic tool with quantitative applicability in biological systems.[10]

In pioneering work, Boxer and co-workers explored the vibrational Stark effect in the liquid phase, leading to the development of the field of vibrational Stark spectroscopy (VSS).[24] Using linear infrared (IR) absorption spectroscopy, Boxer and co-workers demonstrated that several vibrational modes exhibit sensitivity to applied fields,[25,26] with carbonyls and nitriles exhibiting some of the strongest linear responses.[27,28] Because IR-induced vibrations are electric dipole-allowed transitions, the shift of a vibrational frequency relative to zero field ($\Delta\nu_0$) is expressed as a coupling between the transition dipole moment vector and the external field ($\Delta\nu_0 = -\frac{1}{h}\overrightarrow{\Delta\mu}\cdot\vec{E}$).[29,30] In vibrational bioimaging, nitriles are of special interest because they absorb IR light in a frequency region where there is minimal background absorption from native biomolecules (known as the "cell-silent region").[31,32] Thus, nitriles have significant potential for quantitative, intracellular sensing of local electric fields.[33−35]

However, the potential of electric field mapping in cells with nitrile vibrations has not yet been fully realized, mainly due to the limited sensitivity of linear IR absorption spectroscopy.[36] To improve the sensitivity of vibrational bioimaging, a handful of ultrasensitive vibrational microscopy techniques have been developed.[36−41] We recently reported one such technique, termed bond-selective fluorescence-detected IR-excited (BonFIRE) spectro-microscopy (Figure 1).[36] BonFIRE is a picosecond mid-IR (MIR)−near-IR (NIR) double-resonance fluorescence technique (Figure 1b) with applicability to a wide range of fluorescent dyes and excellent biocompatibility. By up-

Received: February 24, 2024
Revised: April 23, 2024
Accepted: April 26, 2024
Published: May 9, 2024

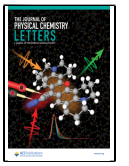




https://doi.org/10.1021/acs.jpclett.4c00597
J. Phys. Chem. Lett. 2024, 15, 5306−5314

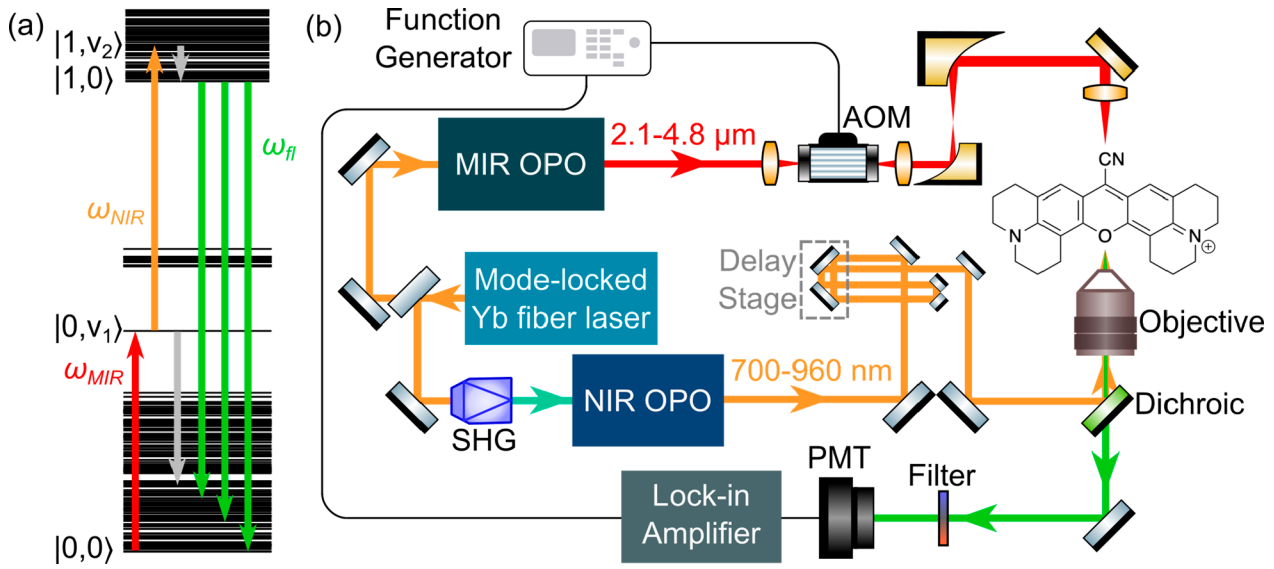


**Figure 1.** Overview of BonFIRE spectroscopy. (a) Jablonski energy level diagram for Rh800. Gray arrows denote vibrational relaxation. Vibronic states are labeled $|E, V\rangle$, where $E$ describes the electronic state and $V$ describes the vibrational state. The energy levels of the Jablonski diagram are the vibrational normal mode manifold of Rh800. (b) BonFIRE instrument diagram (see Section S1 of the SI for full instrumental details). The MIR and NIR beams focus on the structure of Rh800. AOM, acousto-optic modulator; OPO, optical parametric oscillator; SHG, second-harmonic generation; PMT, photomultiplier tube.

converting the vibrationally excited population to a fluorescently active population, BonFIRE achieves single-molecule imaging sensitivity (Figure 1a), drastically increasing the sensitivity of vibrational imaging by allowing for the use of ultrasensitive fluorescence detection schemes.[36]

As a two-pulse experiment, BonFIRE allows for direct measurement of vibrational lifetimes (reflecting the decay of an excited vibrational population) by measuring the decay of fluorescent intensity as a function of the time delay between the MIR and NIR laser pulses.[42−45] Vibrational lifetime measurements provide access to dynamical information, such as site-specific hydration or structural conformation changes in proteins, but accurate lifetime measurements are challenging.[46−49] Until the 1970s, there were no experimental techniques that allowed for direct measurements of liquid-phase vibrational lifetimes, even in pure liquids.[50,51] Historically, lifetimes were inferred from spectral line widths, where lifetime and line width are inversely related by the uncertainty principle. However, measuring lifetimes with linear absorption spectroscopy is challenging for bulk samples in the condensed phase, where inhomogeneous broadening dominates vibrational lineshapes and obscures the homogeneous line width of a transition.[52] For measurements of vibrational lifetimes in biological samples (where inhomogeneous broadening is inevitable and molecular concentration is low), a technique like BonFIRE is necessary because multipulse experiments allow for the measurement of homogeneous lifetimes even in inhomogeneously broadened ensembles.[36,53−56]

In this paper, we investigate the dependence of nitrile vibrational lifetimes on solvation fields by BonFIRE time-domain spectro-microscopy on Rhodamine 800 (Rh800). Originally developed as a laser dye, Rh800 is commercially available, highly photostable, passively permeates cellular membranes, and exhibits minimal cytotoxicity.[57−60] Furthermore, the nitrile of Rh800 is vibronically coupled to its xanthene core and was demonstrated by BonFIRE to have the capability for single-molecule vibrational bioimaging.[36] Through robust convolution fitting and density functional theory (DFT) calculations, we carefully extracted the nitrile lifetimes from our system and proposed a model rationalizing such a dependence, benchmarking the potential of Rh800 nitrile lifetimes to sense local electric fields in biological systems.

Interestingly, we indeed observe a sensitive dependence of the nitrile lifetime of Rh800 in different solvents that are typically adopted for frequency-based VSS (Figure 2a) [see Section S1 of the Supporting Information (SI) for detailed methods and Section S2 for electronic absorption and emission spectra of Rh800; Figure S1].[29] In VSS theory, strongly polar molecules (like nitriles) promote a local alignment of solvent dipoles, leading to the exertion of a net electric field by the solvent on the solute (Figure S2).[61−64] This field, termed the solvent reaction field (SRF), can be quite large in magnitude (∼10 MV/cm), leading to distinctly different vibrational spectra as a function of the solvent (see Section S3 of the SI for further details on SRF theory; eqs S1 and S2).[61,62,65] Given that the effects of electric fields on molecular vibrations are well-documented, we hypothesized that the solvent-dependent lifetimes we observed were also primarily due to the influence of the SRF.

To elucidate the connection between vibrational lifetimes and the SRF, we first need to evaluate the response precision of our picosecond laser system and to robustly retrieve nitrile vibrational lifetimes. An observed signal can be described as the convolution of the instrument response function (IRF) with the molecular response.[66] Because nitrile vibrational decays are generally well-described by a single exponential decay,[31,67] BonFIRE intensity ($I$) as a function of time delay ($t_D$) can be modeled as

$$I(t_D) = \mathrm{IRF} * [H(t_D)e^{-\Gamma t_D}] \quad (1)$$

Here, our IRF is determined by the cross-correlation of our pulses in the time domain,[68] * denotes a convolution, $H(t_D)$ is the Heaviside step function, and $\Gamma$ is the damping rate of the


https://doi.org/10.1021/acs.jpclett.4c00597
J. Phys. Chem. Lett. 2024, 15, 5306−5314

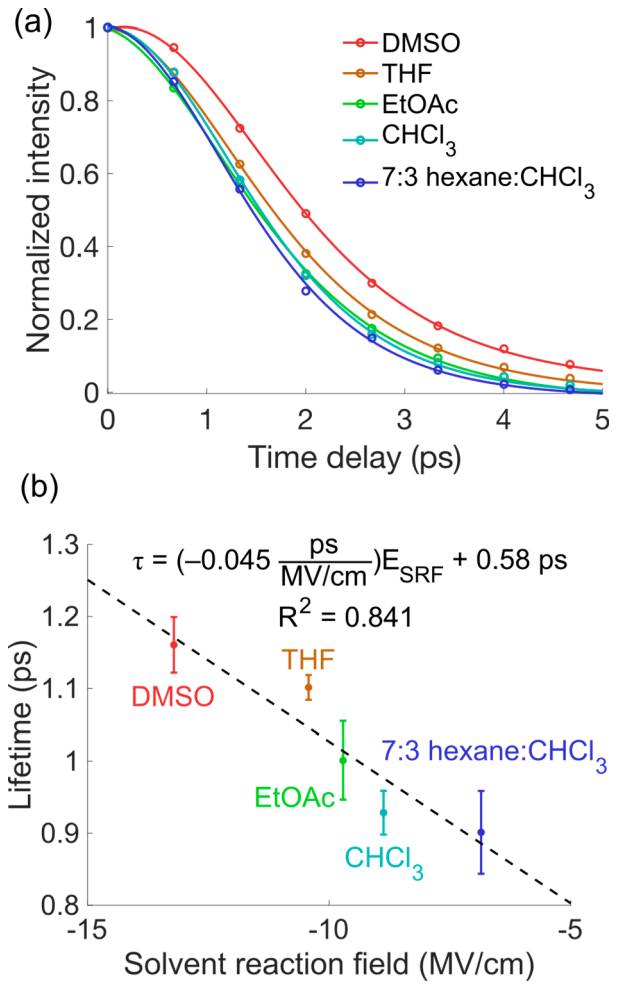


**Figure 2.** Influence of local electric fields on Rh800 nitrile BonFIRE. (a) Data (open circles) and fits to eq 1 (traces) showing the solvent-dependence of BonFIRE time-domain spectra of the nitrile stretch in Rh800 measured at $\omega_{MIR}$ = 2228 cm$^{-1}$, $\lambda_{NIR}$ = 825 nm (pulse width 1.84 ± 0.06 ps, bandwidth 10 cm$^{-1}$). "Normalized intensity" denotes integrated fluorescent intensity collected through a bandpass filter (see Sections S1−S2 of the SI for further details). Raw spectra and fits are provided in Section S7 of the SI (Figure S7). (b) Rh800 nitrile stretch vibrational lifetimes as a function of the solvent reaction field. There is a strong linear correlation ($R^2$ > 0.8) between the lifetime and the SRF, indicating the potential for nitrile vibrational lifetimes to sense local electric fields.

vibrationally excited population (further information can be found in Sections S4 and S5 of the SI; Figures S3 and S4; eqs S3−S10).[69−74] The lifetime ($\tau$) of the vibrationally excited population is defined as $\tau = 1/\Gamma$.[75] This method of data analysis allows for accurate and direct determination of vibrational lifetimes on the picosecond time scale (see Section S6 of the SI for further details; Figures S5 and S6; eqs S11−S14).[76,77]

Fitting of our time-domain data (eq 1) and calculation of the corresponding SRFs (eq S2) allows us to quantitatively assess the dependence of the vibrational lifetime on the local electric field (see Section S7 of the SI for the raw data and equations of the best-fit curves plotted in Figure 2a; Figure S7).[78,79] As plotted in Figure 2b, we see a clear trend of elongation of the vibrational lifetime with increasingly negative SRFs (as was evident from the raw time-domain spectra). Notably, the trend appears to be strongly linear, featuring an adjusted $R^2$ of 0.841 that agrees very well with previous vibrational solvatochromism work on nitrile probes.[29]

As a vibrational lifetime is often considered an intrinsic property of a molecule and not generally subject to change,[68] this first report of the SRF-dependence of a vibrational lifetime could be highly counterintuitive upon first glance. For clues to explain this surprising linear trend, we turned to the extensive body of VSS work in the literature. VSS investigations have primarily focused on the vibrational frequency shifts associated with external electric fields. However, often coincident with the observed shifts in the transition frequency are systematic shifts in the line width of the associated transition.[80] In a homogeneously broadened system, slowing of intramolecular vibrational energy redistribution (IVR; see Section S8 of the SI for details on IVR theory; Figure S8; eqs S15−S18)[75,81−87] by external electric fields manifests as a narrowing of the observed spectral line width, due to elongation of the corresponding vibrational lifetime.[88] For example, Dawlaty and co-workers recently investigated the homogeneous line width alterations in vibrational sum-frequency generation spectroscopy on benzonitrile in applied electric fields,[80] identifying a systematic perturbation of IVR by the external electric field.[88] However, in inhomogeneously broadened systems (like those studied here), lifetimes cannot be directly retrieved from steady-state spectral line widths (see Section S9 of the SI; Figure S9; Table S1; eqs S19 and S20).[36,89,90]

To study the IVR dynamics of Rh800 and understand the linear dependence of nitrile lifetimes on SRFs, we turned to DFT. Since Rh800 is roughly triple the size of prototypical nitrile VSS probes,[27,88] it is significantly more challenging to compute.[23] We first validated our DFT methods [B3LYP, 6-31G(d,p); see Section S1 of the SI for detailed methods][91−93] by comparison to Dawlaty and co-workers' previous DFT vibrational Stark effect study (see Section S10 of the SI for details; Figures S10−S12).[88] From our DFT calculations on Rh800 (see Section S11 of the SI for details; Figures S13−S16), we find strong agreement between predicted IR spectra and experimental data (Figure S13). In varying applied electric fields, we note systematic shifts in the normal-mode frequencies of Rh800 (Figure S14), demonstrating that many of the 162 total normal modes of Rh800 are theoretically sensitive to an external electric field.

IVR is the dominant vibrational relaxation mechanism in polyatomic systems. Though forbidden in a purely harmonic system, mixing of vibrational quanta becomes allowed through anharmonic coupling (see Section S8 of the SI for details). The most common IVR processes are "cubic" or "third order," where the order describes the number of vibrational quanta associated with the process. Higher-order processes are possible but tend to be less probable due to weaker couplings;[94] furthermore, higher-order treatment has previously been demonstrated to be unnecessary for quantitative accuracy in lifetime calculations.[75,85,88] Thus, we limit our analysis to third order here.

To third order, IVR processes can be broadly classified as decays and collisions (Figure S8). A third-order decay describes one quantum of a higher-energy vibration converting into two quanta of lower-energy vibrations, and a third-order collision describes two quanta of lower-energy vibrations converting into one quantum of a higher-energy vibration. For nitrile-stretching vibrations (~2300 cm$^{-1}$), collisional IVR generally requires a CH-stretching acceptor mode (~2900 cm$^{-1}$).[88] Due to the low thermal population of modes above


https://doi.org/10.1021/acs.jpclett.4c00597
J. Phys. Chem. Lett. 2024, 15, 5306−5314

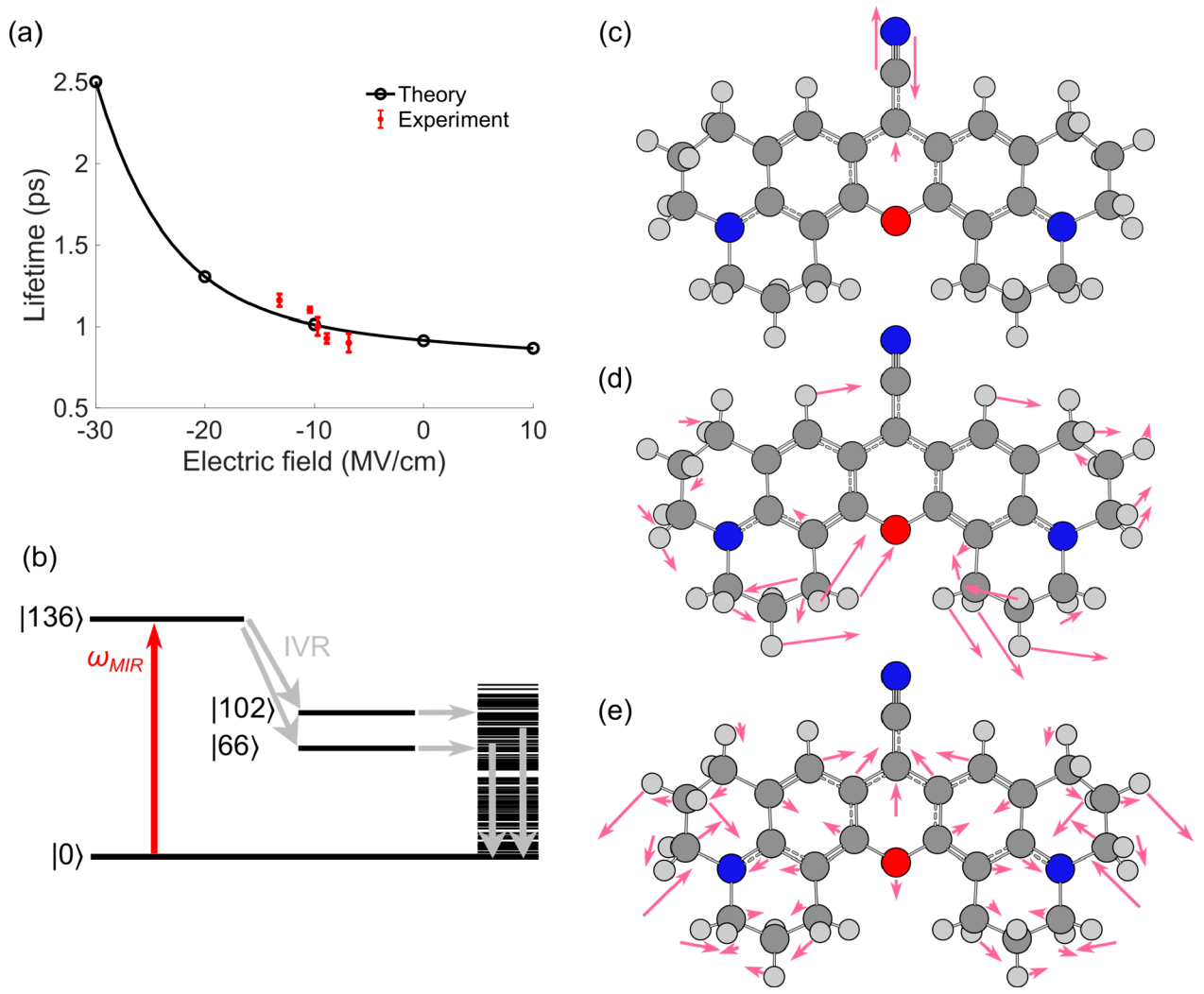


**Figure 3.** IVR lifetime analysis by DFT. (a) Comparison between self-consistent predicted lifetimes by the $\omega_{136} \rightarrow \omega_{102} + \omega_{66}$ IVR pathway (black lines with open circles) and experimentally measured nitrile lifetimes (red dots with error bars). Error bars are ±1 standard deviation. (b) Diagram of energy flow in Rh800 following IR excitation of mode 136, the nitrile-stretching mode. Normal mode displacement vector drawings for modes (c) 136, (d) 102, and (e) 66 (not to scale). Modes 102 and 66 (CH-bending and C═C-stretching modes) serve as the doorway modes that allow for energy from the nitrile stretch to be dissipated into the dense bath of states.

600 $cm^{-1}$ at room temperature, collisional IVR rates (eq S18) were vanishingly small for the nitrile-stretching vibration (mode 136) of Rh800, in agreement with previous nitrile-stretch IVR analysis.[88] We subsequently calculated the decay IVR rates for all of the $162^2$ = 26,244 possible third-order pathways (eq S17).[95−98]

To assign the most probable decay pathway, we first screened our IVR pathways by identifying which pathways were most likely to contribute to the overall decay rate.[75] There are two requirements for efficient IVR: strong anharmonic coupling and the conservation of energy. Qualitatively, the same two requirements apply for a third-order Fermi resonance (TFR; eq S16), allowing TFR to serve as an initial screen of potential IVR pathways. Mode triples with TFR > 1 are said to be "resonantly coupled," indicating a strong possibility of contributing significantly to IVR.[75] For the nitrile stretch of Rh800, we identified 18 IVR pathways that were resonantly coupled over the range of SRFs we studied (Figure S16). Among those 18 decays, we observed that the vibrational lifetimes predicted by the $\omega_{136} \rightarrow \omega_{102} + \omega_{66}$ decay pathway exhibited the strongest agreement with our experimentally measured lifetimes from BonFIRE spectra (Figure 3a). To ensure quantitative accuracy, we iteratively calculated the $\omega_{136} \rightarrow \omega_{102} + \omega_{66}$ IVR rate until the nitrile-stretch damping rate was consistent with the predicted energy transfer rate under zero applied potential (see Section S12 of the SI for details; eqs S21−S23).

For vibrational lifetime predictions at this level of theory, sub-picosecond agreement with experimental data is exceptionally strong (see Section S13 of the SI for numeric values of the data in Figure 3a; Tables S2 and S3).[75] Given this quantitative agreement, we therefore conclude that the $\omega_{136} \rightarrow \omega_{102} + \omega_{66}$ IVR pathway is most reasonable to be the primary decay that we observe in our BonFIRE experiments (Figure 3b). Mode 102 is predominantly a CH-bending (wagging) mode (Figure 3d), and mode 66 is predominantly a C═C-stretching mode, although it also features prominent CH-bending (scissoring) character (Figure 3e). Our results support a growing consensus that nitrile-stretching vibrations in large polyatomic systems generally decay into CH-bending vibrations.[75,88] Importantly, mode 66 contains weak but nonzero nitrile-stretching character (primarily due to strong



https://doi.org/10.1021/acs.jpclett.4c00597
J. Phys. Chem. Lett. 2024, 15, 5306−5314

stretching along the −C−CN bond), making the $\omega_{136} \rightarrow \omega_{102} + \omega_{66}$ IVR pathway intuitively tractable. CH-bending modes are generally very strongly coupled to the dense bath of states.[99,100] Thus, we can construct a diagram of the vibrational energy flow in the nitrile-stretching vibration in Rh800 (Figure 3b), where modes 102 and 66 act as the "doorway" modes that allow the nitrile-stretching vibrational energy to be dissipated into the phonon bath.

Notably, the lifetime trend predicted by the $\omega_{136} \rightarrow \omega_{102} + \omega_{66}$ IVR pathway is not strictly linear with the electric field (see Section S13 of the SI for further details). However, across the range of SRFs that we can generate with traditional solvents, the nitrile vibrational lifetime of Rh800 is appreciably linear with the electric field; hence, local field sensing with linear response should remain valid.[29] These characteristics are consistent with Dawlaty and co-workers' description of the VSS line widths of benzonitrile.[88] Furthermore, slight deviations from linearity have been a hallmark of nitrile vibrational probes since Andrews and Boxer's first reports of VSS with nitriles; most of the vibrational Stark effect can be rationalized as a linear coupling between the dipole moment and the external field, but higher-order terms are needed for a more complete quantitative description of VSS.[28,101,102]

Previous IVR studies of nitrile-stretching vibrations (in benzonitrile and cyanophenylalanine) demonstrated that TFR is strongly correlated with the overall IVR rate.[75,88] Given that TFR (eq S16) is relatively easy to calculate compared to an IVR rate (eqs S17 and S18), TFR thereby served as a convenient metric to assess relative IVR rates. However, our calculations indicate that TFR fails to describe the trend in the nitrile vibrational lifetimes for Rh800. Specifically, $\mathrm{TFR}_{136,102,66}$ decreases with increasingly positive fields (Figure S15), directly contradicting the experimental trend of shorter lifetimes in increasingly positive fields. However, calculation of the corresponding IVR rate ($W_{136,102,66}$; see Section S12 of SI for details) yields quantitative agreement with experimental data (Figure 3a), demonstrating that $\mathrm{TFR}_{136,102,66}$ and $W_{136,102,66}$ predict opposing trends. This failing is notable because it signifies that the vibrational dynamics of the nitrile stretch of Rh800 are appreciably different from those of smaller nitrile probes like benzonitrile and cyanophenylalanine.[75,88]

Although TFR (eq S16) resembles the IVR decay rate (eq S17), we note a few key differences. First, the decay rate depends quadratically on the cubic force constant of a triple of modes, but TFR is linearly dependent on the cubic force constant; it follows that TFR will underestimate the sensitivity of the IVR rate to the degree of anharmonic coupling. Second, we note that the denominator in the TFR term is only the resonance condition but the decay rate includes the resonance condition added with a quadratic damping rate term (due to treatment as a finite-width Lorentzian). As the triple of modes approaches strict resonance ($\Delta\omega = 0$), the TFR term approaches infinity (which can be readily seen in $\mathrm{TFR}_{136,102,66}$; Figure S15), but the IVR rate approaches a finite maximum determined by the intrinsic lifetimes of the modes in the triple; we therefore expect TFR to overestimate the sensitivity of the overall IVR rate to the resonance condition. In support of this reasoning, when we examine the individual components of the $\omega_{136} \rightarrow \omega_{102} + \omega_{66}$ IVR rate equation, we find that the changes we calculate in the IVR rate as a function of the applied electric field are primarily due to changes in the anharmonic coupling (Figure 4; see Figure S17 and Section S14 of the SI for the absolute term contributions).

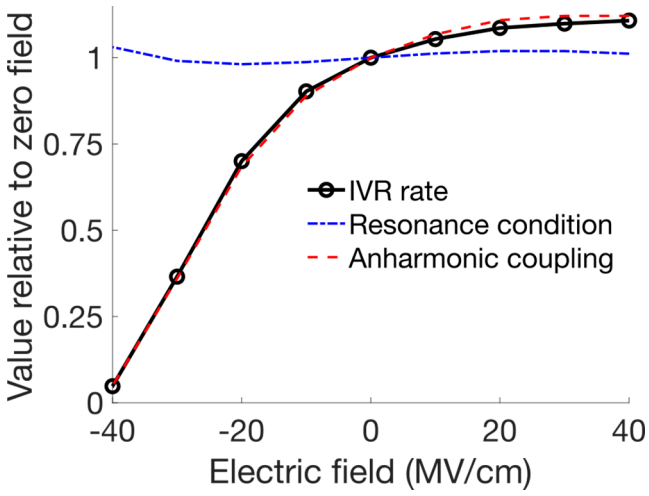


**Figure 4.** Relative IVR rates predicted by the $\omega_{136} \rightarrow \omega_{102} + \omega_{66}$ IVR pathway (black) and contributions from anharmonic coupling (red) and the resonance condition (blue), as calculated by eq S21. Plotted values are standardized relative to their respective values under zero applied field (see Figure S17 for the absolute term contributions). Although the influence of the resonance condition is nonzero, the trend in the IVR rate is dominated by variation in the anharmonic coupling.

Our findings suggest that, for larger molecules like Rh800, anharmonic coupling strength is the dominant factor in IVR efficiency, whereas for smaller molecules like benzonitrile, the dominant factor in IVR efficiency is the resonance condition. This trend can be intuitively understood by considering the scaling of the number of normal modes of a molecule ($3N - 6$ for an $N$-atom, nonlinear molecule). As the number of normal modes increases, the probability of finding a pair of acceptor modes that is approximately resonant with a given donor mode increases as well. Thus, for larger polyatomic molecules like Rh800, pairs of frequency-resonant acceptors are not rare; the limiting factor in IVR thereby becomes the anharmonic coupling strength, and TFRs lose utility as predictors of relative IVR rates (though they do still serve as a useful screen of resonantly coupled mode triples). However, for smaller polyatomic molecules such as benzonitrile with sparser normal mode distributions, finding a pair of resonant acceptors is appreciably less likely; therefore, the resonance condition becomes the limiting factor in the IVR rate for a given vibrational mode, and TFRs remain well-correlated with IVR rates.

We summarize our key findings as follows:

(1) Convolution fitting of BonFIRE time-domain spectra allows highly accurate vibrational lifetime measurements on fluorescent molecules.
(2) The nitrile-stretching (2228 $\mathrm{cm}^{-1}$) vibrational lifetime of Rh800 is strongly correlated ($R^2 = 0.841$) with the solvent reaction field.
(3) Lifetime calculations from DFT yield sub-picosecond agreement with experimental data, allowing us to assign the IVR decay pathway of the nitrile stretch of Rh800.
(4) In larger molecules like Rh800, anharmonic coupling is the limiting factor governing IVR. This trend contrasts with previous IVR analyses on smaller molecules like benzonitrile, where conservation of energy was the limiting factor.


https://doi.org/10.1021/acs.jpclett.4c00597
J. Phys. Chem. Lett. 2024, 15, 5306−5314

Here, we have presented a combined experimental and theoretical investigation of vibrational dynamics in the fluorescent dye Rh800. With double-resonance BonFIRE spectroscopy, we measured vibrational decays in dilute samples on the picosecond time scale, which we analyzed with a thoroughly benchmarked convolution fitting scheme. We observed that the nitrile-stretch vibrational lifetime exhibits a strong linear correlation ($R^2 = 0.841$) with the SRF, laying the foundation for future applications of single-molecule vibrational lifetime sensing with BonFIRE.[36] From DFT calculations, we additionally established a theoretical basis for sensing electric fields with vibrational lifetimes, where the electric field tunes the anharmonic coupling between the vibrational modes of Rh800.

It is worth noting that vibrational lifetime sensing operates on a mechanism different from frequency-shift VSS, potentially offering a new dimension to probe intracellular electrostatics with unparalleled sensitivity when coupled with BonFIRE microscopy. Where VSS is sensitive to the coupling between the external field and the dipole moment of the IR-active mode, vibrational lifetimes are sensitive to the coupling of the field to the IR-active donor mode's transition dipole moment, the acceptor modes' transition dipole moments, and the anharmonic couplings between the modes. Therefore, lifetime sensing theoretically allows for applications inaccessible to frequency-shift-based VSS, such as electric field sensing with a donor vibrational mode that exhibits no Stark shift but does exhibit a lifetime shift from the detuning of its acceptor modes or the associated anharmonic coupling. Although the electric-field dependence established here does not account for lifetime shifts in hydrogen-bonding environments (see Section S15 of the SI for further details; Figure S18), vibrational lifetime imaging in hydrophobic environments, such as liquid−liquid phase-separated condensates, remains a promising future application of local electric field sensing with high sensitivity and quantitative interpretability.

We further demonstrated that lifetime measurements allow for fundamental insights into vibrational dynamics. Through DFT calculations and analysis of IVR rates in a Fermi's golden rule framework, we found sub-picosecond agreement between our experimental lifetimes for the nitrile stretch and the predicted lifetimes from the decay of one quantum of the nitrile stretch into one C═C-stretching quantum and one CH-bending quantum. Our calculations present a disagreement between TFR and IVR rate trends, highlighting that the relative importance of anharmonic coupling versus the resonance condition in the overall IVR rate depends on the normal mode density of the molecular system. These results inform an intuitive, size-based approach to assessing the factors governing vibrational relaxation dynamics in polyatomic molecules.

We expect these experimental and theoretical methods to be broadly generalizable to the study of vibrational dynamics in fluorescent molecules. Although the theoretical methods presented here yield quantitative agreement with experimental results for Rh800, higher levels of theory may be necessary to accurately describe the vibrational dynamics of large polyatomic molecules, in general. We are additionally curious about the generality of sensing local electric fields with nitrile vibrational lifetimes. Our results show that these dynamics are clearly dependent on the molecular structure, but we suspect that these trends are not unique to Rh800 and benzonitrile. Rather, we suspect that there are specific molecular factors (such as being attached to a symmetric, largely nonpolar aromatic scaffold) that predispose a nitrile to having a stronger lifetime response to a local electric field with the ultimate determinant being the coupling between the nitrile and its acceptor modes. Investigations of vibrational dynamics across multiple different classes of dyes to attempt to identify these molecular factors are currently ongoing. By continuing to combine experimental and theoretical approaches, we will further explore vibrational energy flow in large polyatomic molecules, facilitating a much deeper understanding of molecular dynamics and behavior.

## ■ ASSOCIATED CONTENT

### Supporting Information

The Supporting Information is available free of charge at https://pubs.acs.org/doi/10.1021/acs.jpclett.4c00597.

Methods; Rh800 electronic absorption and emission spectra; solvent reaction field theory; theory of BonFIRE spectroscopy; calculation of the instrument response function; simulation of convolution lineshapes and fitting benchmarking; example raw data and fits of BonFIRE time-domain spectra; theory of intramolecular vibrational energy redistribution; inference of Rh800 nitrile lifetimes from steady-state line widths; validation of DFT methods with benzonitrile; Rh800 DFT results; self-consistency of nitrile vibrational lifetime IVR calculations; summary of Rh800 nitrile vibrational lifetimes; absolute term contributions to the assigned IVR decay pathway; vibrational lifetime shifts in protic solvents; references; appendix: code for simulation and fitting of convolution lineshapes (PDF)

Spectral data, fitting simulation results, computed normal-mode frequencies, and nitrile-stretch cubic force constants of Rh800 (XLSX)

Transparent Peer Review report available (PDF)

## ■ AUTHOR INFORMATION


### Corresponding Author

**Lu Wei** − *Division of Chemistry and Chemical Engineering, California Institute of Technology, Pasadena, California 91125, United States;* orcid.org/0000-0001-9170-2283; Email: lwei@caltech.edu

### Authors

**Philip A. Kocheril** − *Division of Chemistry and Chemical Engineering, California Institute of Technology, Pasadena, California 91125, United States;* orcid.org/0000-0002-1265-5931

**Haomin Wang** − *Division of Chemistry and Chemical Engineering, California Institute of Technology, Pasadena, California 91125, United States;* orcid.org/0000-0001-7193-8651

**Dongkwan Lee** − *Division of Chemistry and Chemical Engineering, California Institute of Technology, Pasadena, California 91125, United States;* orcid.org/0000-0001-6091-1349

**Noor Naji** − *Division of Chemistry and Chemical Engineering, California Institute of Technology, Pasadena, California 91125, United States*

Complete contact information is available at: https://pubs.acs.org/10.1021/acs.jpclett.4c00597




https://doi.org/10.1021/acs.jpclett.4c00597
J. Phys. Chem. Lett. 2024, 15, 5306−5314

### Author Contributions

P.A.K., H.W., D.L., and L.W. conceptualized the work. P.A.K. developed and benchmarked the convolution fitting method, performed the DFT calculations, acquired the BonFIRE spectra, and analyzed the data. H.W. and D.L. provided technical guidance. D.L. and N.N. acquired the UV−vis, fluorescence, and FTIR spectra. L.W. supervised the experiments, provided resources, and acquired funding. P.A.K. and L.W. drafted the manuscript. All authors have revised, edited, and given approval to the final version of the manuscript.

### Notes

The authors declare no competing financial interest.

## ■ ACKNOWLEDGMENTS

P.A.K. thanks: Dr. Tomislav Begušić, for patient explanations of theoretical methods; Dr. K.L. Kelvin Lee and Dr. G. Stephen Kocheril, for valuable guidance on a variety of topics, including hardware and software considerations for computational chemistry; Nathanael Kazmierczak and Jax Dallas, for insightful discussions on a variety of topics, including time-domain lineshapes; Anwesha Maitra and Anuj Pennathur, for willingness to assist in the validation of our DFT methods on benzonitrile; Benjamin Spector, for helpful discussions on the nature of energy transfer in molecular systems; Dr. Ryan Leighton, for thorough proofreading of the manuscript; and Dr. Jacob Kirsh, for illuminating discussions on the nature of the vibrational Stark effect. P.A.K. is grateful for financial support from a National Science Foundation Graduate Research Fellowship (DGE-1745301) and a Hertz Fellowship. The computations presented here were conducted with the Resnick High Performance Computing Center, a facility supported by the Resnick Sustainability Institute at the California Institute of Technology. We thank the Caltech Beckman Institute Laser Resource Center for research resources. This work was supported by a National Institutes of Health Director's New Innovator Award (DP2 GM140919-01 for L.W.) and an Alfred P. Sloan Research Fellowship (L.W.). L.W. is a Heritage Principal Investigator supported by the Heritage Medical Research Institute at Caltech.

## ■ REFERENCES

(1) Shaik, S.; Mandal, D.; Ramanan, R. Oriented electric fields as future smart reagents in chemistry. *Nat. Chem.* **2016**, *8*, 1091−1098.
(2) Aragonès, A. C.; Haworth, N. L.; Darwish, N.; Ciampi, S.; Bloomfield, N. J.; Wallace, G. G.; Diez-Perez, I.; Coote, M. L. Electrostatic catalysis of a Diels-Alder reaction. *Nature* **2016**, *531*, 88−91.
(3) Son, Y. W.; Cohen, M. L.; Louie, S. G. Half-metallic graphene nanoribbons. *Nature* **2006**, *444*, 347−349.
(4) Peterka, D. S.; Takahashi, H.; Yuste, R. Imaging voltage in neurons. *Neuron* **2011**, *69*, 9−21.
(5) Hou, J. H.; Venkatachalam, V.; Cohen, A. E. Temporal dynamics of microbial rhodopsin fluorescence reports absolute membrane voltage. *Biophys. J.* **2014**, *106*, 639−648.
(6) Lazzari-Dean, J. R.; Gest, A. M. M.; Miller, E. W. Optical estimation of absolute membrane potential using fluorescence lifetime imaging. *Elife* **2019**, *8*, e44522.
(7) Lin, H.-W.; Mead, G.; Blake, G. A. Mapping LiNbO3 Phonon-Polariton Nonlinearities with 2D THz-THz-Raman Spectroscopy. *Phys. Rev. Lett.* **2022**, *129*, No. 207401.
(8) Fried, S. D.; Wang, L. P.; Boxer, S. G.; Ren, P.; Pande, V. S. Calculations of the electric fields in liquid solutions. *J. Phys. Chem. B* **2013**, *117*, 16236−16248.
(9) Stark, J. Observation of the Separation of Spectral Lines by an Electric Field. *Nature* **1913**, *92*, 401.
(10) Fraser, G. T.; Pate, B. H. The molecular Stark effect in regions of high state density: Overall simplicity and underlying complexity in the response to a static electric field. *J. Chem. Phys.* **1994**, *100*, 6210−6220.
(11) Tamarat, P.; Lounis, B.; Bernard, J.; Orrit, M.; Kummer, S.; Kettner, R.; Mais, S.; Basche, T. Pump-Probe Experiments with a Single Molecule: ac-Stark Effect and Nonlinear Optical Response. *Phys. Rev. Lett.* **1995**, *75*, 1514−1517.
(12) Orrit, M.; Bernard, J.; Zumbusch, A.; Personov, R. I. Stark effect on single molecules in a polymer matrix. *Chem. Phys. Lett.* **1992**, *196*, 595−600.
(13) Marshall, S. A.; Weber, J. Microwave Stark Effect Measurement of the Dipole Moment and Polarizability of Carbonyl Sulfide. *Phys. Rev.* **1957**, *105*, 1502−1506.
(14) Clough, S. A.; Beers, Y.; Klein, G. P.; Rothman, L. S. Dipole moment of water from Stark measurements of H2O, HDO, and D2O. *J. Chem. Phys.* **1973**, *59*, 2254−2259.
(15) Mu, X.; Ye, C.; Zhang, X. Machine-Learning Enhanced Enantioselective Single-Shot-Single-Molecule ac Stark Spectroscopy. *J. Phys. Chem. Lett.* **2023**, *14*, 10067−10073.
(16) Khadria, A. Tools to measure membrane potential of neurons. *Biomed. J.* **2022**, *45*, 749−762.
(17) Suydam, I. T.; Snow, C. D.; Pande, V. S.; Boxer, S. G. Electric fields at the active site of an enzyme: direct comparison of experiment with theory. *Science* **2006**, *313*, 200−204.
(18) Zheng, C.; Mao, Y.; Kozuch, J.; Atsango, A. O.; Ji, Z.; Markland, T. E.; Boxer, S. G. A two-directional vibrational probe reveals different electric field orientations in solution and an enzyme active site. *Nat. Chem.* **2022**, *14*, 891−897.
(19) Zheng, C.; Ji, Z.; Mathews, I. I.; Boxer, S. G. Enhanced active-site electric field accelerates enzyme catalysis. *Nat. Chem.* **2023**, *15*, 1715−1721.
(20) Shi, L.; Hu, F.; Min, W. Optical mapping of biological water in single live cells by stimulated Raman excited fluorescence microscopy. *Nat. Commun.* **2019**, *10*, 4764.
(21) Alonso, J. L.; Pena, I.; Lopez, J. C.; Vaquero, V. Rotational spectral signatures of four tautomers of guanine. *Angew. Chem. Int. Ed.* **2009**, *48*, 6141−6143.
(22) Dutton, S. E.; Blake, G. A. High throughput chirped pulse Fourier-transform microwave spectroscopy of ethanol and water clusters. *Phys. Chem. Chem. Phys.* **2022**, *24*, 13831−13838.
(23) Ratcliff, L. E.; Mohr, S.; Huhs, G.; Deutsch, T.; Masella, M.; Genovese, L. Challenges in large scale quantum mechanical calculations. *WIREs Comput. Mol. Sci.* **2017**, *7*, No. e1290.
(24) Chattopadhyay, A.; Boxer, S. G. Vibrational Stark Effect Spectroscopy. *J. Am. Chem. Soc.* **1995**, *117*, 1449−1450.
(25) Suydam, I. T.; Boxer, S. G. Vibrational Stark effects calibrate the sensitivity of vibrational probes for electric fields in proteins. *Biochemistry* **2003**, *42*, 12050−12055.
(26) Fried, S. D.; Boxer, S. G. Measuring electric fields and noncovalent interactions using the vibrational stark effect. *Acc. Chem. Res.* **2015**, *48*, 998−1006.
(27) Andrews, S. S.; Boxer, S. G. Vibrational Stark Effects of Nitriles I. Methods and Experimental Results. *J. Phys. Chem. A* **2000**, *104*, 11853−11863.
(28) Andrews, S. S.; Boxer, S. G. Vibrational Stark Effects of Nitriles II. Physical Origins of Stark Effects from Experiment and Perturbation Models. *J. Phys. Chem. A* **2002**, *106*, 469−477.
(29) Levinson, N. M.; Fried, S. D.; Boxer, S. G. Solvent-induced infrared frequency shifts in aromatic nitriles are quantitatively described by the vibrational Stark effect. *J. Phys. Chem. B* **2012**, *116*, 10470−10476.
(30) Bagchi, S.; Fried, S. D.; Boxer, S. G. A solvatochromic model calibrates nitriles' vibrational frequencies to electrostatic fields. *J. Am. Chem. Soc.* **2012**, *134*, 10373−10376.
(31) Lindquist, B. A.; Furse, K. E.; Corcelli, S. A. Nitrile groups as vibrational probes of biomolecular structure and dynamics: an overview. *Phys. Chem. Chem. Phys.* **2009**, *11*, 8119−8132.


https://doi.org/10.1021/acs.jpclett.4c00597
J. Phys. Chem. Lett. 2024, 15, 5306−5314

(32) Zhou, L.; Feng, R.-r.; Zhang, W.; Gai, F. Triple-Bond Vibrations: Emerging Applications in Energy and Biological Sciences. *J. Phys. Chem. Lett.* **2024**, *15*, 187−200.
(33) Webb, L. J.; Boxer, S. G. Electrostatic fields near the active site of human aldose reductase: 1. New inhibitors and vibrational stark effect measurements. *Biochemistry* **2008**, *47*, 1588−1598.
(34) Fafarman, A. T.; Boxer, S. G. Nitrile bonds as infrared probes of electrostatics in ribonuclease S. *J. Phys. Chem. B* **2010**, *114*, 13536−13544.
(35) Slocum, J. D.; Webb, L. J. Measuring Electric Fields in Biological Matter Using the Vibrational Stark Effect of Nitrile Probes. *Annu. Rev. Phys. Chem.* **2018**, *69*, 253−271.
(36) Wang, H.; Lee, D.; Cao, Y.; Bi, X.; Du, J.; Miao, K.; Wei, L. Bond-selective fluorescence imaging with single-molecule sensitivity. *Nat. Photonics* **2023**, *17*, 846−855.
(37) Wei, L.; Chen, Z.; Shi, L.; Long, R.; Anzalone, A. V.; Zhang, L.; Hu, F.; Yuste, R.; Cornish, V. W.; Min, W. Super-multiplex vibrational imaging. *Nature* **2017**, *544*, 465−470.
(38) Xiong, H.; Shi, L.; Wei, L.; Shen, Y.; Long, R.; Zhao, Z.; Min, W. Stimulated Raman Excited Fluorescence Spectroscopy and Imaging. *Nat. Photonics* **2019**, *13*, 412−417.
(39) Wang, H.; Lee, D.; Wei, L. Toward the Next Frontiers of Vibrational Bioimaging. *Chem. Biomed. Imaging* **2023**, *1*, 3−17.
(40) Whaley-Mayda, L.; Guha, A.; Penwell, S. B.; Tokmakoff, A. Fluorescence-Encoded Infrared Vibrational Spectroscopy with Single-Molecule Sensitivity. *J. Am. Chem. Soc.* **2021**, *143*, 3060−3064.
(41) Yan, C.; Wang, C.; Wagner, J. C.; Ren, J.; Lee, C.; Wan, Y.; Wang, S. E.; Xiong, W. Multidimensional Widefield Infrared-Encoded Spontaneous Emission Microscopy: Distinguishing Chromophores by Ultrashort Infrared Pulses. *J. Am. Chem. Soc.* **2024**, *146*, 1874.
(42) Laubereau, A.; Seilmeier, A.; Kaiser, W. A new technique to measure ultrashort vibrational relaxation times in liquid systems. *Chem. Phys. Lett.* **1975**, *36*, 232−237.
(43) Whaley-Mayda, L.; Guha, A.; Tokmakoff, A. Multimode vibrational dynamics and orientational effects in fluorescence-encoded infrared spectroscopy. I. Response function theory. *J. Chem. Phys.* **2023**, *159*, No. 194201.
(44) Whaley-Mayda, L.; Guha, A.; Tokmakoff, A. Multimode vibrational dynamics and orientational effects in fluorescence-encoded infrared spectroscopy. II. Analysis of early-time signals. *J. Chem. Phys.* **2023**, *159*, No. 194202.
(45) Mastron, J. N.; Tokmakoff, A. Fourier Transform Fluorescence-Encoded Infrared Spectroscopy. *J. Phys. Chem. A* **2018**, *122*, 554−562.
(46) King, J. T.; Ross, M. R.; Kubarych, K. J. Water-assisted vibrational relaxation of a metal carbonyl complex studied with ultrafast 2D-IR. *J. Phys. Chem. B* **2012**, *116*, 3754−3759.
(47) King, J. T.; Arthur, E. J.; Brooks, C. L., 3rd; Kubarych, K. J. Site-specific hydration dynamics of globular proteins and the role of constrained water in solvent exchange with amphiphilic cosolvents. *J. Phys. Chem. B* **2012**, *116*, 5604−5611.
(48) Lam, Z.; Kong, K. V.; Olivo, M.; Leong, W. K. Vibrational spectroscopy of metal carbonyls for bio-imaging and -sensing. *Analyst* **2016**, *141*, 1569−1586.
(49) Lim, M.; Hamm, P.; Hochstrasser, R. M. Protein fluctuations are sensed by stimulated infrared echoes of the vibrations of carbon monoxide and azide probes. *Proc. Natl. Acad. Sci. U. S. A.* **1998**, *95*, 15315−15320.
(50) von der Linde, D.; Laubereau, A.; Kaiser, W. Molecular Vibrations in Liquids: Direct Measurement of the Molecular Dephasing Time; Determination of the Shape of Picosecond Light Pulses. *Phys. Rev. Lett.* **1971**, *26*, 954−957.
(51) Laubereau, A.; von der Linde, D.; Kaiser, W. Direct Measurement of the Vibrational Lifetimes of Molecules in Liquids. *Phys. Rev. Lett.* **1972**, *28*, 1162−1165.
(52) Laubereau, A.; Kaiser, W. Vibrational Dynamics of Liquids and Solids Investigated by Picosecond Light Pulses. *Rev. Mod. Phys.* **1978**, *50*, 607−665.
(53) Whaley-Mayda, L.; Penwell, S. B.; Tokmakoff, A. Fluorescence-Encoded Infrared Spectroscopy: Ultrafast Vibrational Spectroscopy on Small Ensembles of Molecules in Solution. *J. Phys. Chem. Lett.* **2019**, *10*, 1967−1972.
(54) Schneider, S. H.; Kratochvil, H. T.; Zanni, M. T.; Boxer, S. G. Solvent-Independent Anharmonicity for Carbonyl Oscillators. *J. Phys. Chem. B* **2017**, *121*, 2331−2338.
(55) Cundiff, S. T.; Mukamel, S. Optical multidimensional coherent spectroscopy. *Phys. Today* **2013**, *66*, 44−49.
(56) Yu, Q.; Li, X.; Shen, C.; Yu, Z.; Guan, J.; Zheng, J. Blue-Shifted and Broadened Fluorescence Enhancement by Visible and Mode-Selective Infrared Double Excitations. *J. Phys. Chem. A* **2024**, *128*, 2912−2922.
(57) Alessi, A.; Salvalaggio, M.; Ruzzon, G. Rhodamine 800 as reference substance for fluorescence quantum yield measurements in deep red emission range. *J. Lumin.* **2013**, *134*, 385−389.
(58) Lv, X.; Gao, C.; Han, T.; Shi, H.; Guo, W. Improving the quantum yields of fluorophores by inhibiting twisted intramolecular charge transfer using electron-withdrawing group-functionalized piperidine auxochromes. *Chem. Commun.* **2020**, *56*, 715−718.
(59) Sasaki, S.; Drummen, G. P. C.; Konishi, G.-i. Recent advances in twisted intramolecular charge transfer (TICT) fluorescence and related phenomena in materials chemistry. *J. Mater. Chem. C* **2016**, *4*, 2731−2743.
(60) Sakanoue, J.; Ichikawa, K.; Nomura, Y.; Tamura, M. Rhodamine 800 as a probe of energization of cells and tissues in the near-infrared region: a study with isolated rat liver mitochondria and hepatocytes. *J. Biochem.* **1997**, *121*, 29−37.
(61) Onsager, L. Electric Moments of Molecules in Liquids. *J. Am. Chem. Soc.* **1936**, *58*, 1486−1493.
(62) Sorenson, S. A.; Patrow, J. G.; Dawlaty, J. M. Solvation Reaction Field at the Interface Measured by Vibrational Sum Frequency Generation Spectroscopy. *J. Am. Chem. Soc.* **2017**, *139*, 2369−2378.
(63) Kasyanenko, V. M.; Keiffer, P.; Rubtsov, I. V. Intramolecular vibrational coupling contribution to temperature dependence of vibrational mode frequencies. *J. Chem. Phys.* **2012**, *136*, No. 144503.
(64) Zhu, Q.; Wallentine, S. K.; Deng, G.-H.; Rebstock, J. A.; Baker, L. R. The Solvation-Induced Onsager Reaction Field Rather than the Double-Layer Field Controls CO2 Reduction on Gold. *JACS Au* **2022**, *2*, 472−482.
(65) Luo, Y.; Ågren, H.; Mikkelsen, K. V. Unique determination of the cavity radius in Onsager reaction field theory. *Chem. Phys. Lett.* **1997**, *275*, 145−150.
(66) Kocheril, P. A.; Markus, C. R.; Esposito, A. M.; Schrader, A. W.; Dieter, T. S.; McCall, B. J. Extended sub-Doppler resolution spectroscopy of the $\nu 3$ band of methane. *J. Quant. Spectrosc. Radiat. Transf.* **2018**, *215*, 9−12.
(67) Rodgers, J. M.; Zhang, W.; Bazewicz, C. G.; Chen, J.; Brewer, S. H.; Gai, F. Kinetic Isotope Effect Provides Insight into the Vibrational Relaxation Mechanism of Aromatic Molecules: Application to Cyano-phenylalanine. *J. Phys. Chem. Lett.* **2016**, *7*, 1281−1287.
(68) Maier, J. P.; Seilmeier, A.; Kaiser, W. Population lifetime of CH-stretching modes in medium-size molecules. *Chem. Phys. Lett.* **1980**, *70*, 591−596.
(69) Hamm, P. *Principles of Nonlinear Optical Spectroscopy: A Practical Approach or: Mukamel for Dummies*; University of Zurich: Zurich, Switzerland, 2005.
(70) Li, M.; Razumtcev, A.; Yang, R.; Liu, Y.; Rong, J.; Geiger, A. C.; Blanchard, R.; Pfluegl, C.; Taylor, L. S.; Simpson, G. J. Fluorescence-Detected Mid-Infrared Photothermal Microscopy. *J. Am. Chem. Soc.* **2021**, *143*, 10809−10815.
(71) Bai, Y.; Yin, J.; Cheng, J.-X. Bond-selective imaging by optically sensing the mid-infrared photothermal effect. *Sci. Adv.* **2021**, *7*, eabg1559.
(72) Yoneda, Y.; Kudisch, B.; Rather, S. R.; Maiuri, M.; Nagasawa, Y.; Scholes, G. D.; Miyasaka, H. Vibrational Dephasing along the Reaction Coordinate of an Electron Transfer Reaction. *J. Am. Chem. Soc.* **2021**, *143*, 14511−14522.


https://doi.org/10.1021/acs.jpclett.4c00597
*J. Phys. Chem. Lett.* 2024, 15, 5306−5314

(73) Moya, R.; Kondo, T.; Norris, A. C.; Schlau-Cohen, G. S. Spectrally-tunable femtosecond single-molecule pump-probe spectroscopy. *Opt. Express* **2021**, *29*, 28246−28256.
(74) Whaley-Mayda, L.; Guha, A.; Tokmakoff, A. Resonance conditions, detection quality, and single-molecule sensitivity in fluorescence-encoded infrared vibrational spectroscopy. *J. Chem. Phys.* **2022**, *156*, No. 174202.
(75) Pandey, H. D.; Leitner, D. M. Vibrational States and Nitrile Lifetimes of Cyanophenylalanine Isotopomers in Solution. *J. Phys. Chem. A* **2018**, *122*, 6856−6863.
(76) Kocheril, P. A.; Lenz, K. D.; Mascareñas, D. D. L.; Morales-Garcia, J. E.; Anderson, A. S.; Mukundan, H. Portable Waveguide-Based Optical Biosensor. *Biosensors* **2022**, *12*, 195.
(77) Harper, N.; Hickam, B. P.; He, M.; Cushing, S. K. Entangled Photon Correlations Allow a Continuous-Wave Laser Diode to Measure Single-Photon, Time-Resolved Fluorescence. *J. Phys. Chem. Lett.* **2023**, *14*, 5805−5811.
(78) Weaver, J. B.; Kozuch, J.; Kirsh, J. M.; Boxer, S. G. Nitrile Infrared Intensities Characterize Electric Fields and Hydrogen Bonding in Protic, Aprotic, and Protein Environments. *J. Am. Chem. Soc.* **2022**, *144*, 7562−7567.
(79) Kirsh, J. M.; Weaver, J. B.; Boxer, S. G.; Kozuch, J. Critical Evaluation of Polarizable and Nonpolarizable Force Fields for Proteins Using Experimentally Derived Nitrile Electric Fields. *J. Am. Chem. Soc.* **2024**, *146*, 6983−6991.
(80) Sarkar, S.; Patrow, J. G.; Voegtle, M. J.; Pennathur, A. K.; Dawlaty, J. M. Electrodes as Polarizing Functional Groups: Correlation between Hammett Parameters and Electrochemical Polarization. *J. Phys. Chem. C* **2019**, *123*, 4926−4937.
(81) Maradudin, A. A.; Fein, A. E. Scattering of Neutrons by an Anharmonic Crystal. *Phys. Rev.* **1962**, *128*, 2589−2608.
(82) Uzer, T.; Miller, W. H. Theories of intramolecular vibrational energy transfer. *Phys. Rep.* **1991**, *199*, 73−146.
(83) Kenkre, V. M.; Tokmakoff, A.; Fayer, M. D. Theory of vibrational relaxation of polyatomic molecules in liquids. *J. Chem. Phys.* **1994**, *101*, 10618−10629.
(84) Felker, P. M.; Zewail, A. H. Dynamics of intramolecular vibrational-energy redistribution (IVR). II. Excess energy dependence. *J. Chem. Phys.* **1985**, *82*, 2975−2993.
(85) Leitner, D. M. Mode damping rates in a protein chromophore. *Chem. Phys. Lett.* **2012**, *530*, 102−106.
(86) Stuchebrukhov, A. A.; Kuzmin, M. V.; Bagratashvili, V. N.; Letokhov, V. S. Threshold energy dependence of intramolecular vibrational relaxation in polyatomic molecules. *Chem. Phys.* **1986**, *107*, 429−443.
(87) Fabian, J.; Allen, P. B. Anharmonic Decay of Vibrational States in Amorphous Silicon. *Phys. Rev. Lett.* **1996**, *77*, 3839−3842.
(88) Maitra, A.; Sarkar, S.; Leitner, D. M.; Dawlaty, J. M. Electric Fields Influence Intramolecular Vibrational Energy Relaxation and Line Widths. *J. Phys. Chem. Lett.* **2021**, *12*, 7818−7825.
(89) Wojdyr, M. Fityk: a general-purpose peak fitting program. *J. Appl. Crystallogr.* **2010**, *43*, 1126−1128.
(90) Whiting, E. E. An empirical approximation to the Voigt profile. *J. Quant. Spectrosc. Radiat. Transf.* **1968**, *8*, 1379−1384.
(91) Dalosto, S. D.; Vanderkooi, J. M.; Sharp, K. A. Vibrational Stark Effects on Carbonyl, Nitrile, and Nitrosyl Compounds Including Heme Ligands, CO, CN, and NO, Studied with Density Functional Theory. *J. Phys. Chem. B* **2004**, *108*, 6450−6457.
(92) Hanwell, M. D.; Curtis, D. E.; Lonie, D. C.; Vandermeersch, T.; Zurek, E.; Hutchison, G. R. Avogadro: an advanced semantic chemical editor, visualization, and analysis platform. *J. Cheminform.* **2012**, *4*, 17.
(93) Jacobsen, R. L.; Johnson, R. D., 3rd; Irikura, K. K.; Kacker, R. N. Anharmonic Vibrational Frequency Calculations Are Not Worthwhile for Small Basis Sets. *J. Chem. Theory Comput.* **2013**, *9*, 951−954.
(94) Nesbitt, D. J.; Field, R. W. Vibrational Energy Flow in Highly Excited Molecules: Role of Intramolecular Vibrational Redistribution. *J. Phys. Chem.* **1996**, *100*, 12735−12756.
(95) Yamada, Y.; Katsumoto, Y.; Ebata, T. Picosecond IR-UV pump-probe spectroscopic study on the vibrational energy flow in isolated molecules and clusters. *Phys. Chem. Chem. Phys.* **2007**, *9*, 1170−1185.
(96) West, D.; Estreicher, S. K. First-principles calculations of vibrational lifetimes and decay channels: hydrogen-related modes in Si. *Phys. Rev. Lett.* **2006**, *96*, No. 115504.
(97) West, D.; Estreicher, S. K. Isotope dependence of the vibrational lifetimes of light impurities in Si from first principles. *Phys. Rev. B* **2007**, *75*, No. 075206.
(98) Sakong, S.; Kratzer, P. Hydrogen vibrational modes on graphene and relaxation of the C-H stretch excitation from first-principles calculations. *J. Chem. Phys.* **2010**, *133*, No. 054505.
(99) Yamada, Y.; Ebata, T.; Kayano, M.; Mikami, N. Picosecond IR-UV pump-probe spectroscopic study of the dynamics of the vibrational relaxation of jet-cooled phenol. I. Intramolecular vibrational energy redistribution of the OH and CH stretching vibrations of bare phenol. *J. Chem. Phys.* **2004**, *120*, 7400−7409.
(100) Kayano, M.; Ebata, T.; Yamada, Y.; Mikami, N. Picosecond IR-UV pump-probe spectroscopic study of the dynamics of the vibrational relaxation of jet-cooled phenol. II. Intracluster vibrational energy redistribution of the OH stretching vibration of hydrogen-bonded clusters. *J. Chem. Phys.* **2004**, *120*, 7410−7417.
(101) Błasiak, B.; Ritchie, A. W.; Webb, L. J.; Cho, M. Vibrational solvatochromism of nitrile infrared probes: beyond the vibrational Stark dipole approach. *Phys. Chem. Chem. Phys.* **2016**, *18*, 18094−18111.
(102) Fafarman, A. T.; Sigala, P. A.; Herschlag, D.; Boxer, S. G. Decomposition of vibrational shifts of nitriles into electrostatic and hydrogen-bonding effects. *J. Am. Chem. Soc.* **2010**, *132*, 12811−12813.


https://doi.org/10.1021/acs.jpclett.4c00597
J. Phys. Chem. Lett. 2024, 15, 5306−5314